Estimating Sidereal rotation period of Resident Space Objects using non-uniformly sampled light curves

Katiyayni Balachandran*
University of Texas at Arlington

Dr. Kamesh Subbarao†
University of Texas at Arlington

ABSTRACT

A robust method for the estimation of Sidereal rotation period of Resident Space Objects (RSOs) in orbit using Periodogram analysis is presented. This can be applied to non-uniformly sampled light curves (a measurement of the object's brightness over time), typically used in astronomical data collection. Most ground-based photometric observations are normally non-uniformly spaced due to delegated windows, position of the target and time-delay in information. Other reasons such as weather and diurnal, lunar or seasonal cycles play into effect where sampling is concerned. The Lomb-Scargle Periodogram addresses these issues and is optimal for non-uniformly spaced data with the added benefit of faster computational times. This paper will illustrate the technique in the context of rigid body estimation of asteroids, rocket bodies, and fragments of debris in an ellipsoidal shape. Simulations utilizing uniformly sampled synthetic light curves and those at varying sampling frequencies and angular step-sizes, validate the method within a bounded 10% error for the test cases.

1. INTRODUCTION

Orbital debris exist in large quantities crowding desired orbit regions. Resident Space Objects (RSOs) constitute of natural and artificial objects such as asteroids, active and defunct satellites, spent rocket bodies and debris fragments of varying size [1]. RSOs continue to increase in number and pose potential dangers to other space vehicles from the likelihood of collision. Space object characterization data, such as size and rotational period, can be determined using the detected radiation emitting from the object. Each object in orbit can produce its own light curve, which is a plot of brightness measurements of the astronomical object as seen by the observer versus time. The photometric light curves caused by rotation of a non-spherical RSO has been shown to contain several important pieces of information: one can estimate the sidereal rotation period, spin axis orientation in space, and shape [2]. Typically, a distinguishable feature in a light curve is selected, i.e. maximum or minimum measured brightness or a saddle point, and the re-occurrence of this feature in the light curve can give information on the object's periodicity.

The time it takes for the RSO to rotate about its own spin axis relative to the fixed stars is otherwise known as Sidereal rotation period. For simplicity, this will be referred to as rotation period henceforth in this paper. Various methods have been employed in the past for period determination, of which the following have been discussed below: Epoch method, Fourier series, Phase dispersion minimization and Least-squares analysis.

The Epoch method [2], designed for amateur astronomers, uses multiple light curves and its respective difference in period to compute the spin axis (pole) orientation and direction of rotation. The magnitude of periodic difference is a function of the object's spin axis orientation with respect to the Observer-object-Sun geometry and direction of rotation [3]. In the context of asteroids, not all rotate at the same rate. Therefore, some may require a single light curve spanning several hours to find the period of rotation while others need multiple to observe all facets of geometry. Data collection taken months or years apart sheds light on characteristics of its shape and surface [2]. Composite light

*Graduate Student, Department of Mechanical and Aerospace Engineering, University of Texas at Arlington, Arlington, TX, 76019
†Associate Professor, Department of Mechanical and Aerospace Engineering, University of Texas at Arlington, Arlington, TX, 76019

Copyright © 2018 Advanced Maui Optical and Space Surveillance Technologies Conference (AMOS) – www.amostech.com

curves (obtained through differential CCD photometry) from three or more epochs are fit with a low order Fourier series to determine the fundamental frequency and its corresponding period [4]. Period determination using Phase dispersion minimization [5] distinguishes between possible periods, in which the period producing the least observational scatter about the mean light curve is chosen. It is beneficial for non-sinusoidal light curves where there are scarce observations over a range-bound duration. An optimum light-curve shape is found, which is subtracted from measured data for other periods to be searched.

A similar approach is applied in Lightcurve inversion software [1], written in Fortran by Mikko Kaasaleinen and converted in C by Josef Ďurech [6], that optimizes all parameters and uses spherical harmonics functions for shape models. An initial estimate of the period is input in a parameter file, followed by a period scan. The smallest separation ΔP of local minima in the period parameter space is roughly given by

$$\Delta P \equiv 0.5 \frac{P^2}{\Delta t}$$

where Δt is the full epoch range of the data set. This derives from the fact that the maxima and minima of a double-sinusoidal light curve for periods P and $P \pm \Delta P$ are at the same epochs after Δt. The whole interval of possible periods is scanned to find the global minimum to minimize other parameters.

Unresolved tumbling cylindrical RSOs produce specular and near-specular flashes in identifiable patterns. These are unique to every combination of spin axis vector, phase angle bisector vector and sidereal rotation period for that particular object [7]. A possible range of rotation periods are derived from the average observed flash period. Using brute-force search in the time period of interest, the spin axis vector is optimized using combinations of right ascension and declination values, eliminating ambiguous solutions [2], [7].

Spectral analysis of such photometric observations using the Fast Fourier Transform (FFT) is complex and inadequate with an unevenly spaced dataset. Identifying the true periodicity in a signal then becomes a challenge. Increasing the sampling frequency does mitigate this problem, but by the slightest extent [8]. The large gaps in data impose a problem and require re-sampling and interpolation for uniform spacing [9]. Subsequently, the Power Spectral Density (PSD) estimation is inaccurate, and the additive interpolation noise compromises the computation of the rotation period. Each sampled observation has an associated error variance which multiplies when framing a time series with missing data points.

The above techniques each have constraints on number of data points, spacing intervals or instrumentation used. However, there are other factors influencing the ground-based measured light curves of RSOs such as time of collection and feasibility of observations that affect the accuracy in Period determination. In this paper, a comparative analysis of Fast Fourier Transform and Lomb-Scargle Periodogram is performed with non-uniformly sampled light curves of RSOs. A brief mathematical background for both are illustrated in later sections. A simulation generating synthetic light curves has been designed to test the technique with uniformly-sampled light curves as well.

2. DISCRETE FOURIER TRANSFORM

Consider a continuous function $g(t)$ sampled at regular intervals where the imaginary unit is denoted by $i = \sqrt{-1}$. The Fourier transform is defined as a function of frequency as shown below.

$$\hat{g}(f) \equiv \int_{-\infty}^{\infty} g(t) e^{-2\pi i f t} \mathrm{d}t \tag{1}$$

An infinite time and continuous signal $g(t)$ that is observed at a regular grid with spacing Δt has a Fourier transform that can be written as a Fourier sum rather than its integral form as shown in equation (1). The Fourier Transform of the observed signal is

$$\hat{g}_{obs}(f) = \sum_{n=-\infty}^{\infty} g(n\Delta t) e^{-2\pi i f n \Delta t} \tag{2}$$

[1] http://astro.troja.mff.cuni.cz/projects/asteroids3D/web.php

Copyright © 2018 Advanced Maui Optical and Space Surveillance Technologies Conference (AMOS) – www.amostech.com

Equivalently equation (2) can be re-written as,

$$\hat{g}_{obs}(f) = \sum_{n=0}^{N} g_n e^{-2\pi i f n \Delta t} \tag{3}$$

where g_n, a uniformly-spaced function, is $g_n = g(n\Delta t)$ and $n = 0, 1, 2, ..., N$. Accounting for Nyquist aliasing, the only relevant frequency range is $0 \leq f \leq 1/\Delta t$ [8]. We can then define N evenly-spaced frequencies with $\Delta f = 1/(N\Delta t)$ covering this range.

Denoting $\hat{g}_s \equiv \hat{g}_{obs}(s\Delta f)$, we can re-write equation (3) as

$$\hat{g}_s = \sum_{n=0}^{N} g_n e^{-2\pi i s n/N}$$

which is the standard form of the Discrete Fourier transform (DFT).

The frequency spacing (Δf) of DFT is uniform and favorable in terms of both the Nyquist sampling limit and the finite observing window [8].

3. FAST FOURIER TRANSFORM

The Fast Fourier Transform (FFT) algorithm computes the Discrete Fourier transform (DFT) of a sequence that samples a signal over a period of time and splits it into signals with respective amplitude and phase components at individual frequencies. FFT is widely prevalent in signal processing, specifically for estimating power spectral density (PSD) from time-domain signals.

We denote the Fourier Transform operator as $F\{g\} = \hat{g}(f)$ and to eliminate the complex components and remove the phase, we square the amplitude of the resulting transform which is commonly known as the power spectral density (PSD) or power spectrum, $PSD_g \equiv |F\{g\}|^2$. PSD is a positive real-valued function of the frequency f that distinguishes each individual frequency that is present in the total signal.

FFT is advantageous due its to high processing speeds and reduces the complexity from $O(n^2)$ to $O(n \log n)$ where n is the data size. Linearity of the transform means that the Fourier transform directly measures periodic content in a continuous function since the signal is made up of a sinusoidal components [8]. However, it does require uniformly-spaced data which is not always the case with astronomical data pertaining to Space objects.

In order to get evenly sampled data, interpolation and resampling need to be performed which creates inaccuracies in PSD estimation [9].

4. NON-UNIFORM SAMPLING

Uniformly spaced data obtained in intervals are analyzed by standard Fourier methods (based on Fast Fourier Transform) as well as the Method of Maximum Entropy [10]. Most astronomical ground-based observations do not contain uniformly spaced data due to delegated windows for data collection, position of the object under observation and time-delay of information. Other reasons such as weather and diurnal, lunar or seasonal cycles play into effect where sampling is concerned [8].

In the generic non-uniform case, a signal is measured N times and the set is represented by $\{t_n\}$. The observed signal is a function of the true signal $g(t)$ and the observing window $W_{\{t_n\}}(t)$ [8],

$$g_{obs}(t) = g(t) W_{\{t_n\}}(t)$$

where the window is represented by a sum of Dirac delta functions.

$$W_{\{t_n\}}(t) = \sum_{n=1}^{\infty} \delta(t - t_n)$$

Copyright © 2018 Advanced Maui Optical and Space Surveillance Technologies Conference (AMOS) – www.amostech.com

The Dirac delta function δ is denoted below.

$$\delta(t-t_n) = \frac{1}{2\pi}\sum_{n=-\infty}^{\infty} e^{ip(t-t_n)}dp$$

Thus,

$$g_{obs}(t) = g(t)\sum_{n=1}^{\infty}\delta(t-t_n)$$

and taking its Fourier Transform, essentially from the convolution of transforms.

$$F\{g_{obs}\} = F\{g\} \circledast F\{W_{\{t_n\}}\} \tag{4}$$

The Power spectrum of a non-uniformly sampled signal is more complex than uniform observations. The spectrum of a uniformly spaced dataset has a unique period since the frequency at the highest peak is distinguishable from surrounding peaks. The Fourier transform of the non-uniformly spaced delta functions looks like random noise. There is a direct correlation between the random observation times and the random Fourier peaks (amplitude and position on the spectrum). Therefore, non-structured spacing of observations will lead to non-structured frequency peaks in the window transform, and when convolved with the Fourier transform of the underlying signal also produces the same random noise [8].

Due to aliasing, there are other peaks of varying heights created by each true peak in the spectrum. Only one period can be computed at a time using the major peak of the spectrum to avoid errors [10]. Subsequent periods have to be found by successively subtracting the previously found periodicities from the data and regenerating new spectrums with the added noise. Generically, with unequally spaced data, the properties of the Fourier Transform are inadequate. Considering the simplest noise-free data with a singular sinusoidal frequency, the chances of getting the highest peak at the right position is slim. Increasing the sampling frequency does mitigate this problem, but by the slightest extent [8].

The method both optimal and frequently used to calculate the Power spectrum of non-uniformly sampled data is Periodogram analysis. It ignores the non-equal spacing and calculates the normal Fourier power spectrum, as if the data were equally spaced without using the same approach as FFT. Periodogram analysis provides a reasonably good approximation to the spectrum obtained by fitting sine waves by least-squares to the data and plotting the reduction in the sum of the residuals against frequency [10].

5. PERIODOGRAM

Classical Periodogram

Applying the definition of the Power spectrum to the Discrete Fourier Transform defined previously, and multiplying it by a factor of $1/N$ results in the Classical periodogram [8].

$$P_C(f) = \frac{1}{N}\left|\sum_{n=1}^{N} g_n e^{-2\pi i f t_n}\right|^2 \tag{5}$$

Primarily, the Classical periodogram is optimal for the uniform sampling case as it is able to capture all the frequency components. While the periodogram follows the definition of the power spectrum, conceptually, the former is an estimator of the latter. These terms are used interchangeably in the astronomy community. Extensions of the Classical periodogram (such as the Lomb-Scargle Periodogram which will be discussed later) have intrinsic variances in cases even where there are infinite number of observation points [8].

Copyright © 2018 Advanced Maui Optical and Space Surveillance Technologies Conference (AMOS) – www.amostech.com

We can expand and re-write equation (5) using Euler's Theorem to eliminate complex variables.

$$\begin{aligned} P_C(f) &= \frac{1}{N}\left|\sum_{n=1}^{N} g_n[\cos(-2\pi f t_n) + i\sin(-2\pi f t_n)]\right|^2 \\ &= \frac{1}{N}\left|\sum_{n=1}^{N} g_n[\cos(2\pi f t_n) - i\sin(2\pi f t_n)]\right|^2 \\ &= \frac{1}{N}\left[\left(\sum_{n=1}^{N} g_n\cos(2\pi f t_n)\right)^2 + \left(\sum_{n=1}^{N} g_n\sin(2\pi f t_n)\right)^2\right] \end{aligned} \tag{6}$$

While the Classical periodogram is useful for identifying periodic signals from non-periodic, for a case of non-uniform sampling, the periodogram is harder to distribute using a Chi-squared term [8]. A more generalized form took its place and is known as the Lomb-Scargle Periodogram to ensure that it holds this property.

Lomb-Scargle Periodogram

The Lomb-Scargle Periodogram, combined several properties such that it was able to simplify to the Classical form for equally-spaced data, and is not influenced by global time-shifts in the observations. The difference lies in the proportionality multiplied by each term, no longer $1/N$ which is expected for complete phase sampling at each frequency [8]. The Periodogram function is expressed below:

$$P_{LS}(f) = \frac{1}{2}\left\{\frac{(\sum_n g_n\cos(2\pi f[t_n-\tau]))^2}{\sum_n \cos^2(2\pi f[t_n-\tau])} + \frac{(\sum_n g_n\sin(2\pi f[t_n-\tau]))^2}{\sum_n \sin^2(2\pi f[t_n-\tau])}\right\} \tag{7}$$

where τ is defined for each frequency f so that time-shift invariance is non-existent:

$$\tau = \frac{1}{4\pi f}\arctan\left(\frac{\sum_n \sin(4\pi f t_n)}{\sum_n \cos(4\pi f t_n)}\right)$$

Lomb-Scargle Periodogram ensures accuracy for non-uniform sampling provided that the data has uncorrelated white noise [8].

6. RESULTS & SIMULATION

Computing the Sidereal rotation period is trivial once the periodogram analysis is completed. From the spectrum, the frequency at which the highest peak occurs is defined as f_0 and subsequently, the rotational period about its own spin axis is $T = \frac{1}{f_0}$. Test cases of RSOs of both uniformly and non-uniformly sampled light curves have been taken and their resulting Fourier Transforms and Lomb-Scargle Periodograms (plotted in MATLAB) are shown below.

Asteroid 3122 Florence

3122 Florence is classified as a near-Earth object and potentially hazardous asteroid. Using the Asteroid Lightcurve Photometry Database (ALCDEF)[2], the light curve of 3122 Florence whose observations where gathered between January 2016 to October 2017 is shown below. It is assumed that the observation points have been calibrated for the apparatus and require no further processing.

[2] http://alcdef.org/alcdef_GenerateALCDEFPage.php

Copyright © 2018 Advanced Maui Optical and Space Surveillance Technologies Conference (AMOS) – www.amostech.com

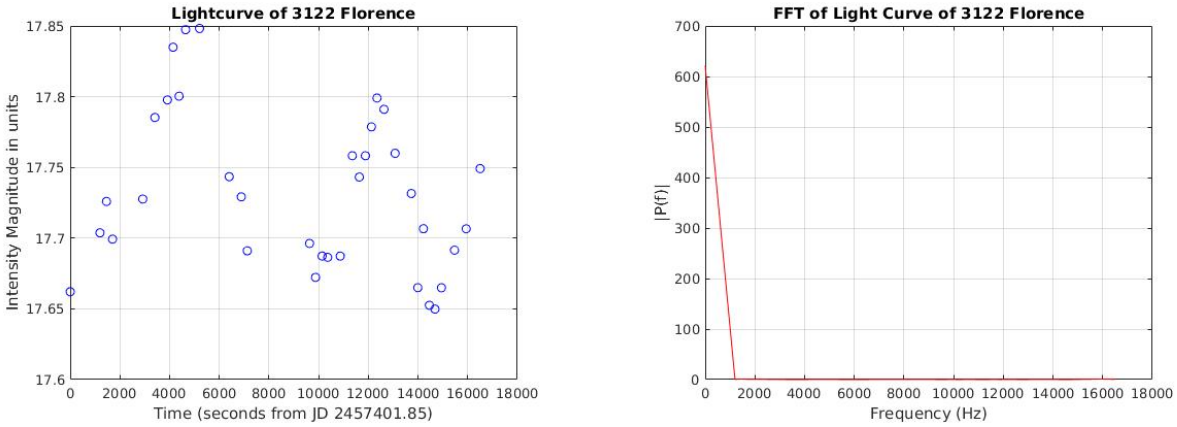

(a) Light curve of 3122 Florence

(b) Fast Fourier Transform of light curve

Figure 1: 3122 Florence: Light curve (Left) and FFT (Right)

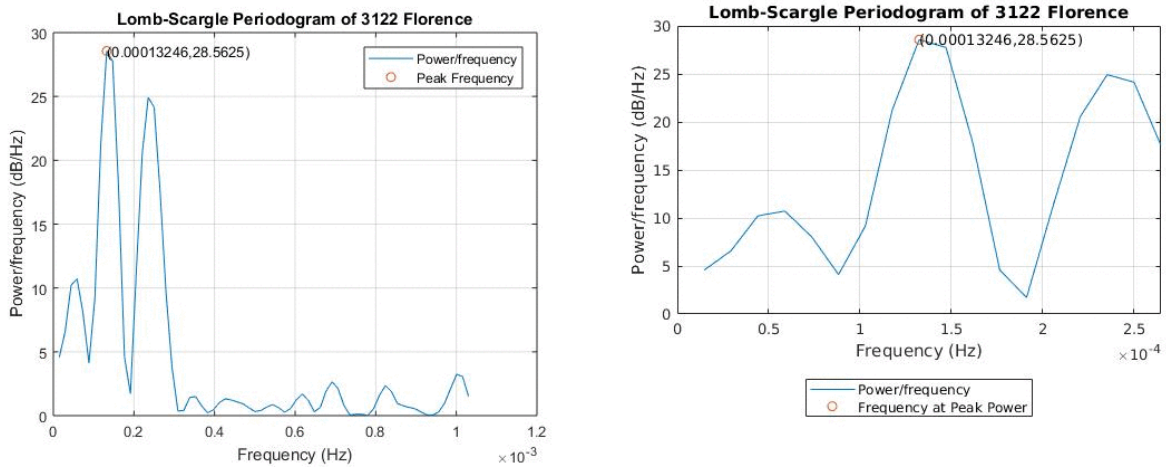

Figure 2: (Left) Lomb-Scargle Periodogram of light curve, (Right) Zoom in view of Lomb-scargle Periodogram centered at Rotational frequency

The FFT (Fig. 1b) shows the fundamental frequency f_0 at 0 Hz which is incorrect. This verifies that Fourier Transform is not applicable with non-uniformly sampled light curves. Instead, employing the Lomb-Scargle Periodogram, the non-zero rotation frequency f is annotated (Fig. 2 Right) as 0.00013246 Hz. The computed Sidereal rotation period is $T = 2.0970$ hrs whereas the reference literature value is 2.3580 hrs [11]. There is approximately an 11% deviation from the expected. Many factors can contribute to this, one of which being human error in precision of data collection from a plot[3]. If the data has a lot of gaps, the additive interpolation noise affects the calculation of rotation period.

Asteroid 43 Ariadne

43 Ariadne is a sizeable main-belt asteroid. The relative light curve points were obtained from the test file in Database of Asteroid Models from Inversion Techniques (DAMIT) Lightcurve Inversion software[4] and the best solution generated through convex optimization is $T = 5.761985$ hrs and a spin pole orientation of $\lambda = -15°$, $\beta = 253°$. The appropriate light curve and its Lomb-Scargle periodogram is depicted in Fig. 3 and 4 respectively.

[3] https://www.mathworks.com/matlabcentral/fileexchange/64194-grabit-polyfit

[4] https://astro.troja.mff.cuni.cz/projects/asteroids3D/web.php?page=download_software

Copyright © 2018 Advanced Maui Optical and Space Surveillance Technologies Conference (AMOS) – www.amostech.com

As noted in Fig. 4 (right), the peak frequency f_0 is at 9.6914 x $10^{-}5$ Hz. The rotation period is calculated to be 2.8877 hrs. This is approximately half of the expected value and is a phenomenon sometimes visible with elongated asteroids. Most asteroids are irregularly shaped so that the projected area of the surface facing the Sun varies as the asteroid rotates [4]. The light curve (almost symmetric) will generally have two minima and two maxima per period. An oblong object rotating about a spin axis (tilted to non-zero angles with respect to both its major and minor body axes) shows an increasing projected area to the observer until it reaches a maximum. Then the projected area decreases to a minimum, followed by another maximum as the object completes a full turn. The time between adjacent maxima is therefore half the rotational period [4]. The half-period is the most promiment period in the data when using any period analysis technique, hence the actual period of rotation is $2T$. The computed sidereal rotation period of 43 Ariadne is 5.7754 hrs, generating a minuscule 0.23% error.

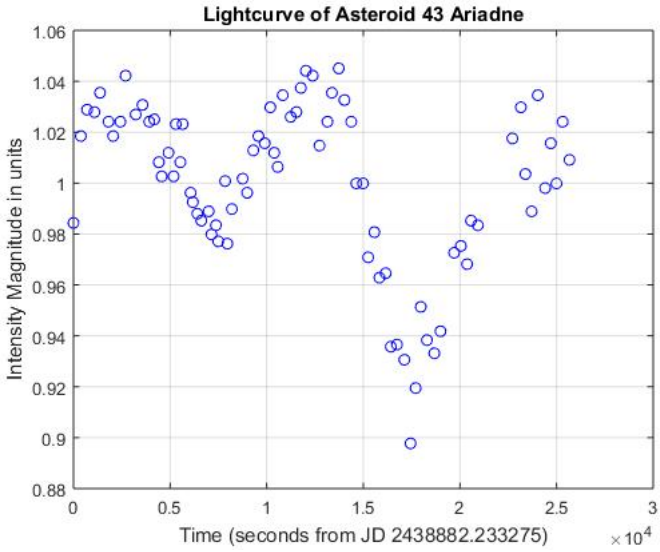

Figure 3: Light curve of Asteroid 43 Ariadne

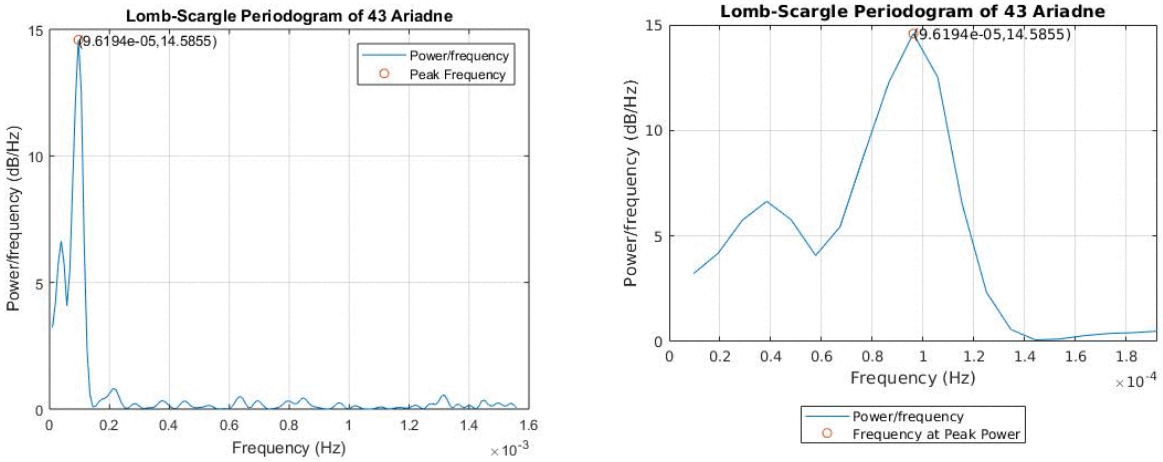

Figure 4: (Left) Lomb-Scargle Periodogram of 43 Ariadne, (Right) Zoom in view of Lomb-scargle Periodogram centered at Rotational frequency

The light curve databases predominantly found online are for asteroids, small planets and some moons. However, artificial satellites are rare to come across for peer-access, unless specificially commissioned. Any observations made by other researchers are welcome to validate this technique. Instead, synthetic light curves can be generated and this

Copyright © 2018 Advanced Maui Optical and Space Surveillance Technologies Conference (AMOS) – www.amostech.com

is described in the following section.

Simulation of 43 Ariadne

Using the 3D vertex coordinates of 43 Ariadne generated from the Database of Asteroid Models from Inversion Techniques (DAMIT) software suite written by Joseph Dŭrech, and applying Delauney triangulation gives us the facets on the shape model (Fig. 5).

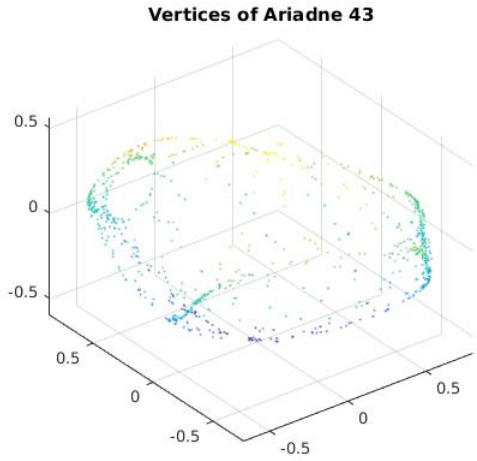

(a) Vertices Point cloud

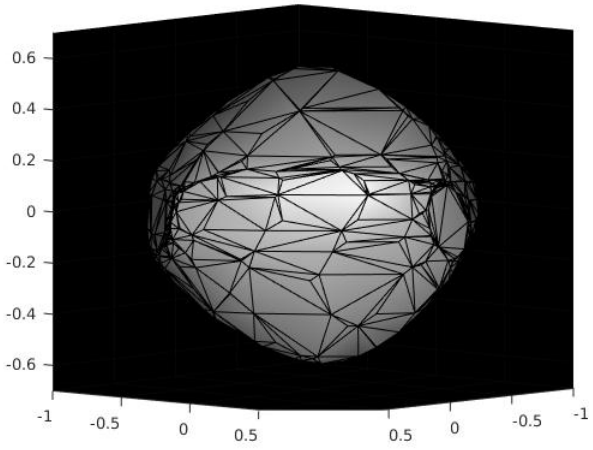

(b) Surface Triangulation

Figure 5: 43 Ariadne as seen by the observer at 0°

The surface reflectance properties were set to include ambient, diffuse and specular reflection ($k_a = 0.5,\ k_d = 1,\ k_s = 0.3$ respectively)[5]. The motion of the sun with respect to the asteroid is negligible and assumed constant. The lighting conditions are ideal to produce uniform white light at a point source that radiates in all directions. The astrocentric coordinates of the Sun at the first observed Julian date are $(1.467574,\ 1.309298,\ 0.08242228)$ AU. The light is interpolated linearly across each triangular facet using the vertex normals. Similarly, the observer's location on earth has

[5] http://paulbourke.net/miscellaneous/asteroid/

Copyright © 2018 Advanced Maui Optical and Space Surveillance Technologies Conference (AMOS) – www.amostech.com

the astrocentric coordinates of $(0.7140329,\ 0.6399864,\ 0.0723648)$ AU and is facing the target. Since this RSO is resolved, we are aware of its ecliptic pole coordinates as $\lambda = -15^\circ,\ \beta = 253^\circ$. Permuting rotations about this spin axis orientation such that each rotation takes about 1 *ms* has the results tabulated below.

The object was simulated to make a rotation of some arbitrary angle approximately every millisecond as it completed 1 full rotation 360° about its own spin axis. The results from varying angle step-size of rotation have been listed below to show the accuracy of the Lomb-Scargle Periodogram in both uniform and non-uniform cases.

Table 1: Half-periods of Ariadne after varying angle step-size and their simulation errors

Angle step-size (°)	Computed Half-Period (s)	Expected Half-Period (s)	Error (%)
0.5	0.3891	0.36	8.1
1.5	0.1167	0.12	2.8
2	0.0882	0.09	2.0
5	0.0380	0.036	5.6
7	0.0276	0.0257	7.4
9	0.0234	0.02	17.0
15	0.0125	0.012	4.2

From Table 1, we can conclude that computed half-period through Lomb-Scargle Periodogram is a reasonable estimate within 10% error with one outlier at step-angle of 9 degrees. The light curves and their associated periodograms are illustrated for comparison in Table 2.

Copyright © 2018 Advanced Maui Optical and Space Surveillance Technologies Conference (AMOS) – www.amostech.com

Table 2: Table of uniformly-sampled synthetic light curves of 43 Ariadne and periodograms at different angle step-sizes (Top to Bottom: 0.5°, 1.5°, 2°, 5°, 9°)

(Left to Right) Step-Angle, Light curve, Lomb-Scargle Periodogram, Zoom-in view of L-S Periodogram			
0.5°	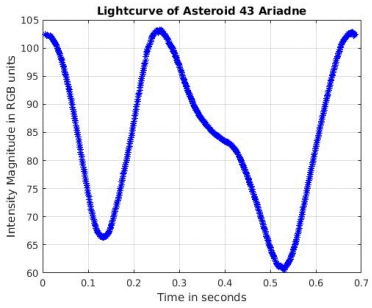	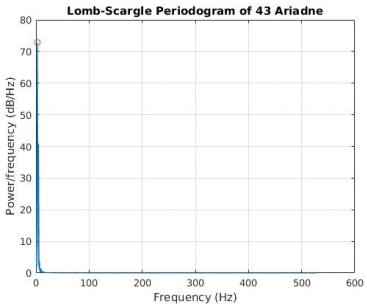	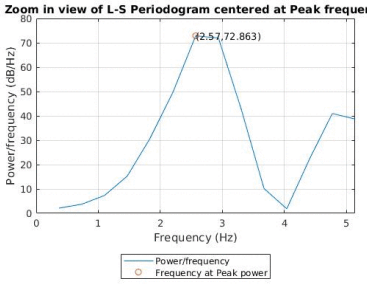
1.5°	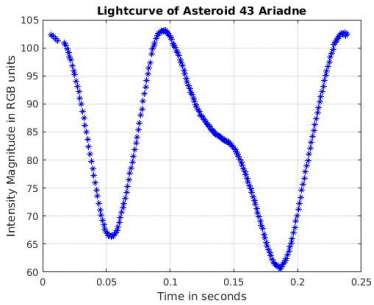	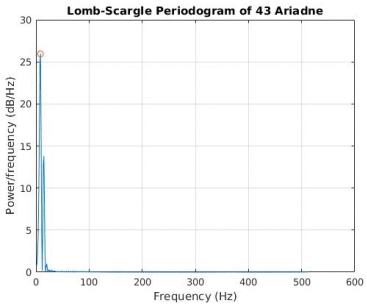	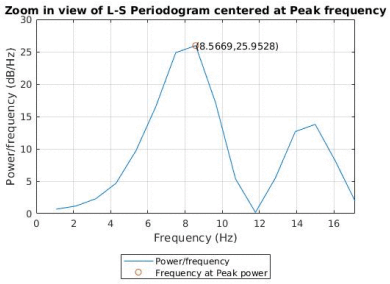
2°	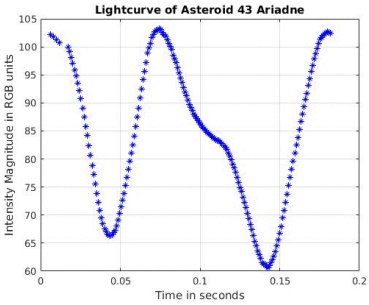	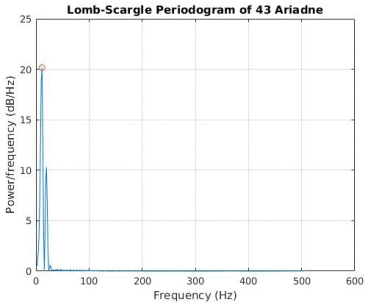	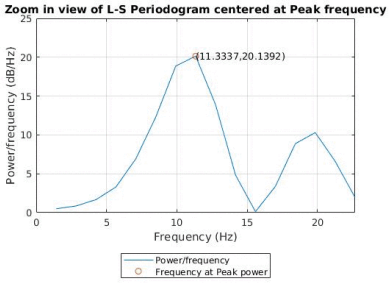
5°	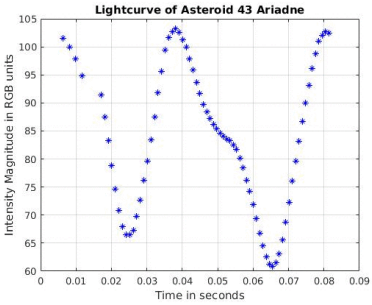	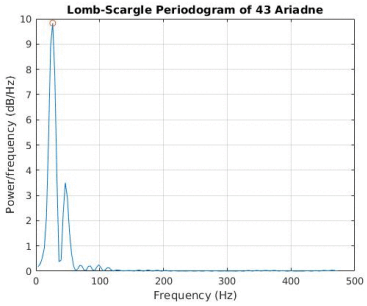	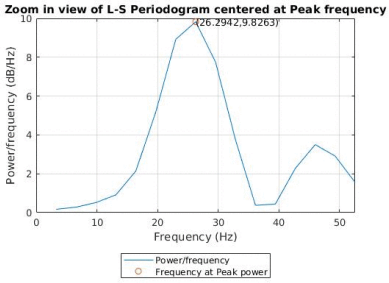
9°	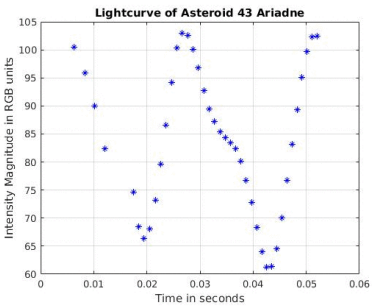	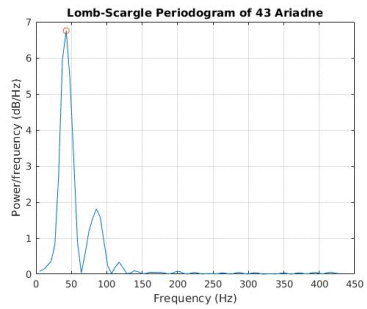	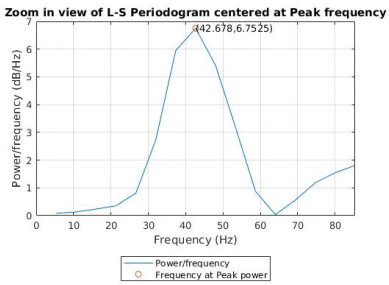

Copyright © 2018 Advanced Maui Optical and Space Surveillance Technologies Conference (AMOS) – www.amostech.com

Although the zoom-in views of the Lomb-Scargle Periodogram in Table 2 show comparable shapes, their peaks occur at different rotational frequencies, hence the period of rotation varies as well.

Simulation using Rocket Nose Cone

Using the CAD model[6] of a rocket nose cone, we can generate synthetic light curves by specifying the position of observer and target parameters along with material surface properties.

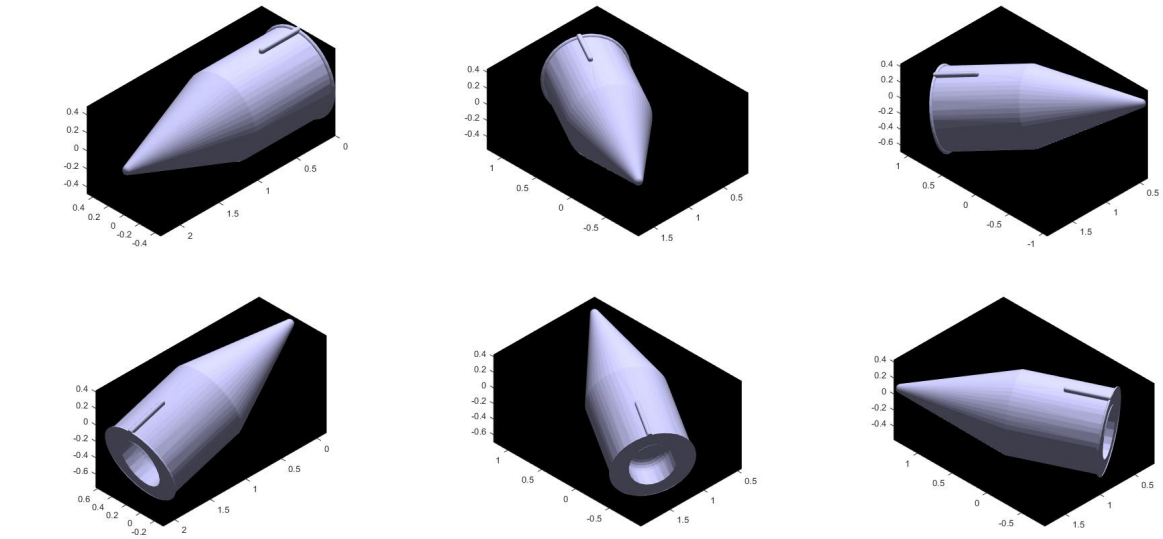

Figure 6: Different geometries of Rocket nose cone at specified angles of rotation as seen by the observer.
1st Row: (Left to Right) 60°, 120°, 180°, 2nd Row: (Left to Right) 240°, 300°, 360°

The material surface properties were set to include ambient, diffuse and specular reflection ($k_a = 0.8,\ k_d = 0.1,\ k_s = 1$ respectively). Rocket nose cones are primarily made of plastic, fiberglass and hard wood[7], hence the choices of reflective properties. The lighting conditions are ideal to produce uniform white light at a point source that radiates as a headlight. The position of the object with respect to the observer's location on earth has the coordinates of $(0.7140329,\ 0.6399864,\ 0.0723648)$ AU, identical to 43 Ariadne. The spin axis orientation is user-defined as $\lambda = -20°,\ \beta = 90°$. Tumbling effects are ignored in this scenario. Performing rotations about the spin axis such that each rotation takes about 1 *ms* has the results seen below in Table 3.

Table 3: Rotation period of Rocket nose cone at varying angle step-size and number of rotations along with their simulation errors

Number of 360° Rotations	Angle step-size (°)	Computed Period (s)	Expected Period (s)	Error (%)
1	1	0.3256	0.36	9.6
1	2	0.1506	0.16	5.9
1	5	0.0659	0.072	8.5
0.5	1	0.3351	0.36	6.9
2	1	0.3192	0.36	11.3
3	1	0.3172	0.36	11.9

[6] C. Kaufman
[7] T. Beach, http://www.unm.edu/~tbeach/IT145/week05/parts.html

Copyright © 2018 Advanced Maui Optical and Space Surveillance Technologies Conference (AMOS) – www.amostech.com

Table 4: Table of uniformly-sampled synthetic light curves of the Rocket nose cone and periodograms at different number of 360-degree rotations and constant angle step-size of 1°

Number of full-rotations	Light curve	Lomb-Scargle Periodogram
0.5	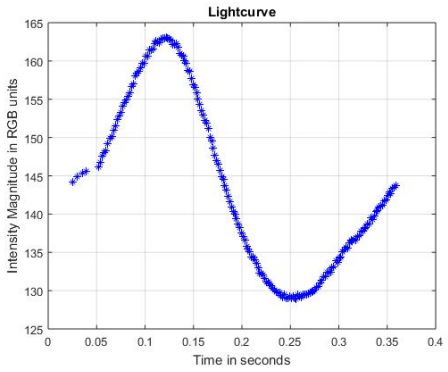	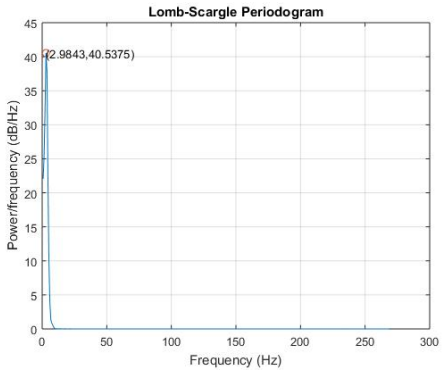
1	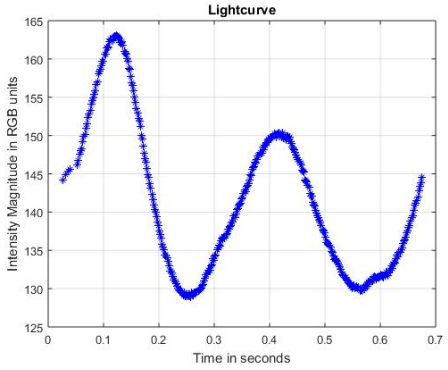	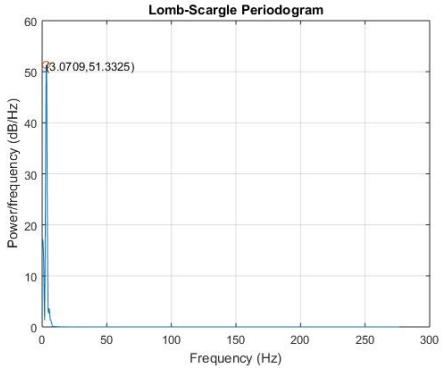
2	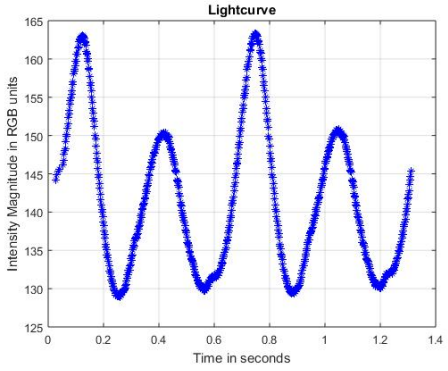	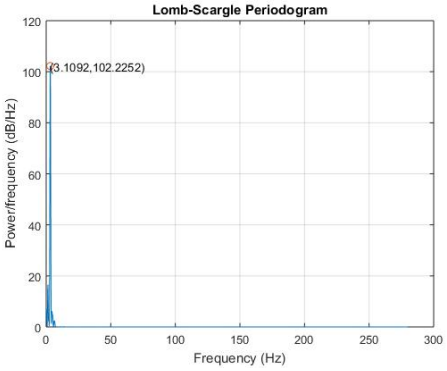
3	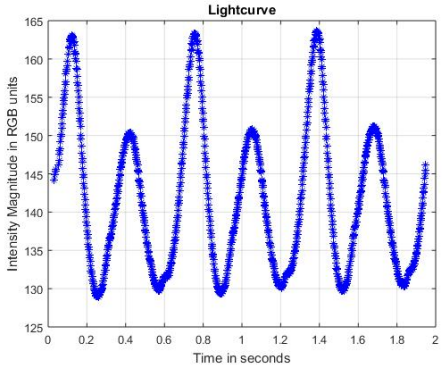	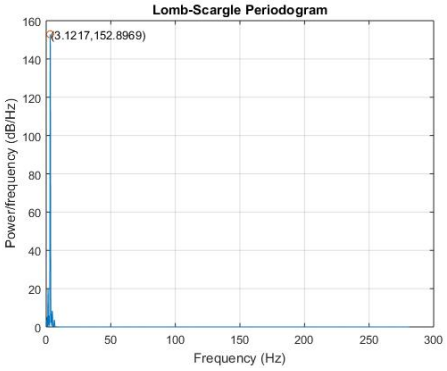

Copyright © 2018 Advanced Maui Optical and Space Surveillance Technologies Conference (AMOS) – www.amostech.com

The object was simulated to make a rotation of some arbitrary angle approximately every millisecond as it completed k full 360° rotations about its own spin axis. The results from varying angle step-size of rotation and k rotations have been tabulated in Table 3 to show the accuracy of the Lomb-Scargle Periodogram. The period can be calculated directly, rather than its half-period since it is not an irregularly shaped asteroid.

For a single full-angular rotation, the computed periods at differing angle step-sizes are reasonable estimates of the expected values, within a 10% bounded error. It is observed in Table 3 that as the number of rotations increase, the accuracy decreases such that the deviation is larger. Regardless of the period of time of data collection for a step-size of 1°, the Lomb-Scargle periodograms have peaks occurring at relatively close frequencies as seen in Table 4.

This validates the consistency of results and re-assures that the window of data collection is irrelevant to determine the Period of rotation. These values are dependent on the previously stated test case parameters and may differ for other spin axis orientations. Since there is little to no access to available "truth" values with which to compare these results, the paper invites observations and analyses from other researchers to validate this technique and verify the Sidereal rotation periods determined through simulation means.

7. CONCLUSIONS & FUTURE WORK

The results obtained confirm that the Lomb-Scargle Periodogram is a good estimator to determine the Sidereal rotation period using light curves of RSOs and the cohesiveness in simulation results show that the derived values are authentic. While the Fast Fourier Transform is appropriate for unifomly-sampled light curves, it is not applicable to non-uniformly spaced observations. This causes a defficiency in its effectiveness as a period determination approach. It was shown that the Lomb-Scargle Periodogram is accurate in both scenarios, making it the optimal choice for ground-based astronomical observations. Although the simulation was able to replicate the motions of Asteroid 43 Ariadne, it is noticeable that the presence of errors exists and increases slightly for an angle step-size of 9 degrees. Elongated objects produce half-periods with the Periodogram analysis due to the presence of symmetric light curves with two maxima and minima.

Spent rocket bodies and defunct satellites are major sources of orbital debris that need to be removed. The tested Rocket nose cone showed consistent results when changing the duration of data collection at constant angle step-sizes, making this technique reliable. Future work includes testing with light curves of operational and inactive satellites. Artificial RSOs are complex in that they have distinct regions of changing reflectance, unlike asteroids. This needs to be explored since there is currently an approximation using the Bidirectional Reflectance Distribution Functions (BRDF). With numerous RSOs, investigations to gather light curve data will corroborate the approach described in this paper. Once the period is determined, more information such as pole orientation and its attitude can aid towards the object's classification in the Space catalog. A generic method may be developed for unknown targets that exhibit periodic changes in brightness and give forth to estimating its shape and motion solely based on photometric observations and astrometric data using ground-based data collection methods.

8. REFERENCES

[1] Shai Segal, Pini Gurfil, and Kamran Shahid. In-orbit tracking of resident space objects: A comparison of monocular and stereoscopic vision. *IEEE Transactions on Aerospace and Electronic Systems*, 50(1):676–688, 2014.

[2] W Wild. Estimating asteroid pole orientation from photometric light curves. *International Amateur-Professional Photoelectric Photometry Communications*, 68:14, 1997.

[3] T Yanagisawa and H Kurosaki. Shape and motion estimate of leo debris using light curves. *Advances in Space Research*, 50(1):136–145, 2012.

[4] John C Armstrong, B Nellermore, and L Reitzler. Measuring rotation periods of asteroids using differential ccd photometry. *International Amateur-Professional Photoelectric Photometry Communications*, 63:59, 1996.

[5] Robert F Stellingwerf. Period determination using phase dispersion minimization. *The Astrophysical Journal*, 224:953–960, 1978.

Copyright © 2018 Advanced Maui Optical and Space Surveillance Technologies Conference (AMOS) – www.amostech.com

[6] Josef Ďurech, Benoît Carry, Marco Delbo, Mikko Kaasalainen, and Matti Viikinkoski. Asteroid models from multiple data sources. In *Asteroids IV*, pages 183–201. The University of Arizona Press, 2015.

[7] Phil Somers. Cylindrical rso signatures, spin axis orientation and rotation period determination. In *Advanced Maui Optical and Space Surveillance Technologies Conference*, 2011.

[8] Jacob T VanderPlas. Understanding the lomb–scargle periodogram. *The Astrophysical Journal Supplement Series*, 236(1):16, 2018.

[9] Pablo Laguna, George B Moody, and Roger G Mark. Power spectral density of unevenly sampled data by least-square analysis: performance and application to heart rate signals. *IEEE Transactions on Biomedical Engineering*, 45(6):698–715, 1998.

[10] Nicholas R Lomb. Least-squares frequency analysis of unequally spaced data. *Astrophysics and space science*, 39(2):447–462, 1976.

[11] Brian D Warner. Near-earth asteorid lightcurve analysis at cs3-palmer divide station: 2016 january-april. *Minor Planet Bulletin*, 43:240–250, 2016.

Copyright © 2018 Advanced Maui Optical and Space Surveillance Technologies Conference (AMOS) – www.amostech.com